ELSEVIER

Journal of Molecular Catalysis A: Chemical 122 (1997) 175–186

JOURNAL OF MOLECULAR CATALYSIS A: CHEMICAL

On the nature of acid sites in substituted aluminophosphate molecular sieves with the AEL topology

Daniel Arias [a], Iván Campos [a], Douglas Escalante [a], José Goldwasser [a], Carmen M. López [*, a], Francisco J. Machado [a,*], Bernardo Méndez [a], Delfin Moronta [a], Mariela Pinto [a], Virginia Sazo [a], M.M. Ramirez de Agudelo [b]

[a] *Centro de Catálisis, Petróleo y Petroquimica, Facultad de Ciencias, UCV, Apdo. 47102, Caracas 1020-A, Venezuela*
[b] *INTEVEP, S.A., Apdo. 76343, Caracas 1070-A, Venezuela*

Received 4 December 1996; accepted 10 January 1997

Abstract

A series of substituted $AlPO_4$ molecular sieves with the AEL topology were prepared and characterized by different techniques, to evaluate the amount and nature of the additional elements and their effect on the acidity and catalytic properties of the resulting solids. It was found that a one-to-one interaction between Lewis (L) and Brønsted (B) sites occurs after calcination of the substituted materials, leading to an enhanced acidity and causing, as a result, an increase in the selectivity towards isobutene during the transformation of 1-butene. Substitution models are discussed in order to rationalise the origin and nature of such B–L synergism.

Keywords: Substituted $AlPO_4$; Acidity; Molecular sieves; 1-butene transformation; Acid-sites nature

1. Introduction

The origin and nature of acid sites in substituted $AlPO_4$ molecular sieves has not yet been completely understood in spite of the large amount of work done. Topological models for the incorporation of silicon in the aluminophosphate framework and its consequence on the acidity properties of the resulting SAPO have been advanced [1–3]. In this case acid sites have been associated to the environment of Si atoms in the $AlPO_4$ framework, their strength and density being a function of the relative distribution of Si(nAl) species with 'n' ranging from zero to 4. For metal-substituted $AlPO_4$ the acidity has been ascribed to the incorporation of divalent metals in place of Al sites [4]. However higher metal oxidation states have been observed in metal-containing $AlPO_4$ such as CrAPO, having relatively strong acid sites. A model, based on a structural defect generated by the formation of dioxochromium (VI) species in the framework of CrAPO-5 after the calcination [5], has been advanced to explain this behaviour. An analogous proposal, based on the

* Corresponding authors. Fax: +58-2-19797037 or 6052136; e-mail: fmachado@strix.ciens.ucv.ve or cmlopez@strix.ciens.ucv.ve.

PII S1381-1169(97)00028-9

occurrence of defective oxochromium (V) in chromosilicate with the ZSM-5 structure, has also been reported [6].

Isobutene is the starting material for the industrial production of methyl tertiary-butyl ether (MTBE) that is at present, and will probably be in the near future, the primary oxygenated octane booster to compensate for the reduction of lead and aromatics and to meet the oxygen requirement of the reformulated gasolines. The skeletal isomerization of *n*-butenes has become a very attractive route to isobutene. Medium-pore molecular sieves such as zeolites ferrierite [7] and ZSM-22 [8] and substituted aluminophosphates with the AEL [4] and ATO [9] topology have been tested as catalysts for this molecular rearrangement. Two different models considering either a bi-molecular mechanism involving the dimerization of *n*-butenes to octenium-like ions as the initial step, followed by branching and cracking to isobutene [10] or a direct isomerization of *n*-butenes through a monomolecular route [8] have recently been proposed to occur over ferrierite and ZSM-22, respectively. A series of Me-AlPO-11 were also proved to be highly selective and stable catalysts for this transformation [4]. A monomolecular mechanism was suggested by these authors with the participation of weakly acidic OH-groups interacting with Lewis acid centres as the active sites.

The main purpose of this paper is to study the modes of acidity generation and the nature of the resulting acid sites, after the incorporation of different additional elements in the aluminophosphate framework. In order to evaluate the effect of such compositional changes on the catalytic behaviour, the transformation of 1-butene at 743 K is used as a test.

2. Experimental

2.1. Sample preparation and characterization

A detailed synthesis procedure for the preparation of $AlPO_4$-11 and SAPO-11 was given in a previous paper [3]. Cr-containing samples were prepared by adding an aqueous chromium (III) hydroxiacetate solution to the synthesis gel under synthesis conditions similar to those used for the AEL-like preparation, Fe and Mn were introduced in the synthesis gel as $FeSO_4 \cdot 7H_2O$ and $Mn(CH_3COO)_2 \cdot 4H_2O$, previously dissolved in the phosphoric acid solution. Typical synthesis conditions of the solids studied are given in Table 1, together with their corresponding nomenclature as used in this work. A sample of SAPO-11 was impregnated with chromium by incipient wetness using the same source of chromium.

Al and P contents of the solids were determined with the aid of an atomic emission spectrometer, having a source of plasma inductively coupled. Si content was analyzed by atomic emission spectrometry. The percentage of crys-

Table 1
Synthesis conditions and nomenclature of the solids studied

Solid	Nomenclature used in this work	Gel molar composition	T_c (K)	t_c (h)
SAPO-11A	S-11A	Al_2O_3:P_2O_5:0.3SiO_2:DPA:50H_2O	473	24
SAPO-11B [a]	S-11B	Al_2O_3:P_2O_5:0.3SiO_2:DPA:50H_2O	473	24
$AlPO_4$-11	A-11	Al_2O_3:P_2O_5:DPA:50H_2O	473	24
Cr/SAPO-11B	Cr/S-11B	Cr-impregnated on SAPO-11B	—	—
FAPO-11	F-11	0.9Al_2O_3:P_2O_5:0.2FeO:DPA:50H_2O	473	24
MnAPO-11	Mn-11	0.9Al_2O_3:P_2O_5:0.2MnO:DPA:50H_2O	423	72
CrAPO-11	Cr-11	0.9Al_2O_3:P_2O_5:0.06Cr_2O_3:DPA:50H_2O	423	90
CrAPSO-11	CrS-11	0.9Al_2O_3:P_2O_5:0.06Cr_2O_3:DPA:50H_2O:0.3SiO_2	423	90

T_c and t_c: temperature and time of crystallization, respectively.
DPA: di-*n*-propylamine; Et_3N: triethylamine.
[a] Time of gel preparation before crystallization was halved with respect to SAPO-11A preparation.

tallinity was determined from the X-ray diffractograms recorded, after calcination of the synthetic solids overnight at 773 K, with a Philips diffractometer PW 1730 using Co-Kα radiation ($\lambda = 1.790255$ Å) operated at 30 kV, 20 mA and a scanning speed of 2° 2θ/min. Diffraction lines between 8 and 25° 2θ were taken as reference for this calculation. The sample S-11A, showing the highest summation of the XRD-line intensities, was used as the reference pattern. N_2-specific surface areas (SSA) were obtained with a Micromeritics 2200 sorptometer at liquid nitrogen temperature, after pre-treating the samples in situ at 623 K under vacuum for 3 h. ^{57}Fe Mössbauer spectra were taken at room temperature using a ^{57}Co/Pd source and fitted by a non-linear least-square regression program. X-band EPR spectra were recorded at room temperature with a Varian line-E spectrometer. Diffuse reflectance (DRS) spectrum of CrAPO was recorded with a UV-VIS Perkin-Elmer spectrometer, scanning from 200 to 800 nm at a rate of 100 nm/cm and chart speed of 50 nm/cm, using alumina as a white reference.

NMR experiments were performed with the aid of two different instruments, a Bruker AMX and a MSL spectrometers, both of them operated at 300 MHz for ^{1}H, 121.44 MHz for ^{31}P and 78.17 MHz for ^{27}Al. The spinning rate ranged between 8 and 10 KHz. Single pulses of 3.3 μs were applied for ^{31}P and ^{27}Al runs. ^{1}H–^{27}Al CP/MAS NMR spectra were recorded using a single contact pulse sequence, 1000 μs contact time, 90° ^{1}H-pulse and 4 s recycle delay. Chemical shifts of ^{27}Al and ^{31}P are given in ppm from external $Al(H_2O)_6^{+3}$ and 85% H_3PO_4, respectively.

2.2. Catalytic test

The transformation of 1-butene was carried out at 743 K under atmospheric pressure by feeding a mixture of 1-butene/N_2 in a molar ratio of 0.25 and overall gas flow rate of 60 cm^3 min^{-1}, to a stainless-steel continuous flow reactor containing 1 g of catalyst. The product analysis was done after 30 min on-stream by on-line gas chromatography, using a Hewlett-Packard 5890 chromatograph equipped with a fused silica KCl/Al_2O_3 capillary column and a FID detector. The skeletal isomerization efficiency (SIE) was defined as the fractional approach to the normalised isobutene equilibrium concentration (46.7%), excluding 1-butene, at 743 K. The catalytic parameters were evaluated from the corrected chromatographic areas for each product (A_i), excluding the reactant 1-butene, as follows:

(1) Conversion (X):

$$X = \left[\sum A_i / \left(\sum A_i + A_{1\text{-butene}} \right) \right] \quad (1)$$

(2) Selectivity (S_i):

$$S_i = \left[A_i / \sum A_i \right] \times 100 \quad (2)$$

(3) Skeletal isomerization efficiency (SIE):

$$\text{SIE} = \left[\frac{A_{\text{iso-butene}}}{(A_{\text{iso-butene}} + A_{\text{cis-2-butene}} + A_{\text{trans-2-butene}})} \right] \times \frac{1}{0.467} \quad (3)$$

The following selectivities were determined: S_{si} (skeletal isomerization), S_{db} (double bond isomerization), S_b (formation of butadiene), S_{C5+}, (formation of hydrocarbons from C_5 to C_8), S_c (formation of hydrocarbons from C_1 to C_3). S_{C5+} and S_c were calculated by introducing the summation of the corresponding corrected areas in the numerator of Eq. (2).

2.3. Acidity measurement

Surface acidity was characterized by FTIR of the pyridine/catalyst interaction. Self-supporting wafers of 7 mg/cm^2 were placed in a IR-cell specially designed for gas and thermal 'in situ' treatments and activated under vacuum (10^{-5} Torr) at 723 K overnight. Afterwards, the temperature was dropped to 363 K and pyridine was admitted to the cell (5 Torr). Then, the excess pyridine was evacuated. All the spectra

in the pyridine region were recorded after outgassing at 443, 623 and 723 K. The intensity of the bands (band area/wafer optic density) at 1550 and 1450 cm^{-1} measured after each outgassing temperature, were taken to be proportional to the concentration of Brønsted and Lewis acid sites, respectively. For the purpose of this work three distinct acidity regions were arbitrarily defined in terms of the acid strength: total acidity (weak + moderate + strong) related to those sites retaining pyridine at 443 K, moderate + strong acidity, ascribed to those sites retaining pyridine at 623 K and strong acidity, associated with those sites retaining pyridine at 723 K.

3. Results and discussion

3.1. Characterization

Some characteristics of the solid studied are given in Table 2. The N_2-sorption capacity of all of them is fairly good, with SSA values within the range previously reported for these structures [11]. Observed differences can not be attributed to variations of the crystal integrity of the solids since, for instance, the sample S-11A having a relatively low SSA value showed a degree of crystallinity of 100%. Moreover, the sample F-11 with the lowest crystallinity presented a high sorption capacity. Therefore, there is not a clear correlation between these two parameters as could be expected. Probably, in the former case, some extra-framework material remaining from the synthesis, undetected by XRD, might be present in the pore channels causing a reduction of its sorption capacity.

Table 2
Some characteristics of the solids studied

Sample	SSA (m^2/g)	% Cryst.	Molar composition formula TO_2
S-11A	90	100	$(Al_{0.48}P_{0.47}Si_{0.05})O_2$
S-11B	124	70	$(Al_{0.47}P_{0.47}Si_{0.06})O_2$
A-11	116	100	$(Al_{0.5}P_{0.5})O_2$
Cr/S-11B	114	70	$(Al_{0.47}P_{0.42}Si_{0.06}Cr_{0.05})O_2$
F-11	149	52	$(Al_{0.46}P_{0.5}Fe_{0.04})O_2$
Mn-11	87	65	$(Al_{0.47}P_{0.5}Mn_{0.04})O_2$
Cr-11	95	—	$(Al_{0.52}P_{0.45}Cr_{0.03})O_2$
CrS-11	151	100	$(Al_{0.50}P_{0.43}Cr_{0.03}Si_{0.05})O_2$

Table 3
Brønsted (B) and Lewis (L) acid strength distribution

Sample	B-band intensity			L-band intensity		
	443 K	623 K	723 K	443 K	623 K	723 K
S-11A	1.96	1.51	1.46	2.72	2.29	0.80
S-11B	3.32	3.29	3.29	3.83	2.86	2.61
A-11	3.40	0	0	4.59	2.72	2.60
Cr/S-11B	8.28	3.10	2.02	5.59	3.83	1.30
F-11	1.74	1.09	0	7.93	1.12	0
Mn-11	2.97	1.90	0	2.47	2.10	0
Cr-11	3.43	3.38	2.03	4.59	4.28	2.21
CrS-11	5.35	4.54	3.40	4.86	4.85	3.08

The molar fraction of the additional element lies between 0.04 and 0.08. ^{29}Si MAS NMR technique has previously been used to verify the incorporation of Si in the AEL framework [3].

Acid strength distribution is presented in Table 3 for both Brønsted an Lewis acid sites. As seen, the presence of an additional element in the basic aluminophosphate solid generates a significant increase in the Brønsted acid strength, strongly suggesting its incorporation in the framework. Surprisingly the basic $AlPO_4$-11 showed weak Brønsted acidity. No explanation, other than attributing this behaviour to structural defects leading to terminal P-OH and Al-OH groups, has been found. The occurrence of moderate and strong Lewis sites on this solid supports the idea of structural breakage after calcination to yield defective Al sites as follows:

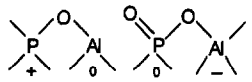

Obviously, these Al sites would not interact with charge-compensating protons which can not be present due to the lack of additional charge-unbalancing elements in the framework.

The incorporation of Si generates a relatively high proportion of strong Brønsted acid sites. It

is apparent from Table 3 that the sample S-11A contains lower acid site density than its analogous S-11B. However, when the total B-band intensity (at 443 K) was divided by the product of the SSA and the fractional Si content, values of 0.44 and 0.45 Brønsted units/m^2 Si-atom, were respectively obtained. This result clearly reveals that pyridine accessibility to the pore system of the sample S-11A is reduced, supporting our previous suggestion in the sense that some pore-plugging by extra-framework material, should be occurring. Furthermore, this result also indicates that each Si atom in the framework generates the same amount of Brønsted acidity, as should be expected for structures with similar Si loading obtained by the same mechanism of Si incorporation.

Incorporation of metals also yield solids of higher acid strength. In the case of the Mn-containing sample the model advanced by Gielgens et al. [4] seems to rationalise the surface acidity observed for this solid. According to this model, depicted in Fig. 1, divalent metals would be incorporated into the AEL framework generating one P–OH group for each metal ion. Metal ions would act as Lewis sites interacting with Brønsted P–OH entities. The occurrence of Mn(II) was evidenced from the X-band EPR spectrum taken at room temperature, showed in Fig. 2. Thus, the typical 6 major lines associated with Mn(II) species are clearly observed from Fig. 2a. In order to resolve this sextet of hyperfine lines a sample with a significantly lower Mn content (0.1 wt%) than the one used for the catalytic test (7.2 wt%) had to be analyzed. A Mn-supported $AlPO_4$-11 sample of the same composition (0.1 wt%) showed no resolution of

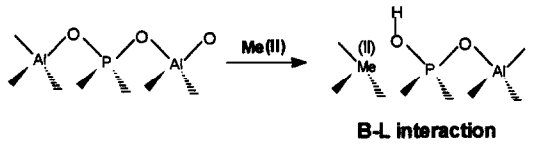

Fig. 1. Model by Gielgens et al. [4] explaining the way divalent ions like Mn^{2+} generate surface acidity. A Brønsted–Lewis interaction is apparent.

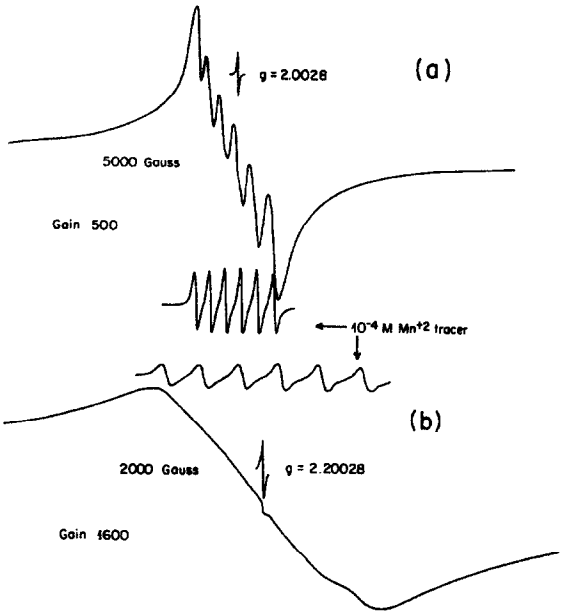

Fig. 2. X-band EPR spectrum of (a) MnAPO-11 and (b) Mn-supported $AlPO_4$-11 with about 0.1 wt% of Mn.

these lines, as shown in Fig. 2b, suggesting a better Mn dispersion on the former.

^{31}P MAS NMR spectra for Mn-11 and a Mn-impregnated $AlPO_4$-11 (Mn/$AlPO_4$-11) are

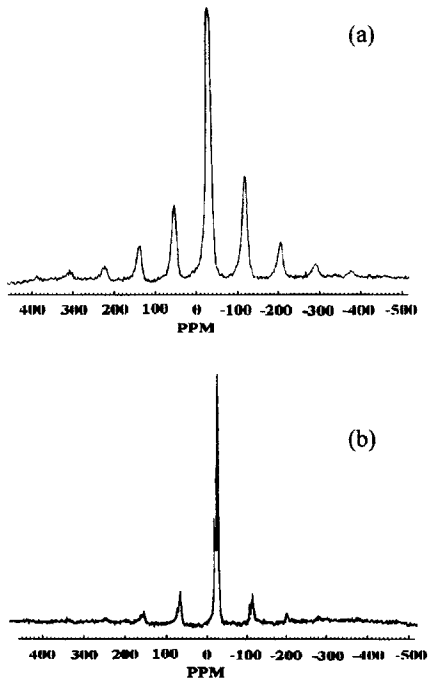

Fig. 3. ^{31}P MAS NMR spectra of the calcined solids (a) Mn-11 and (b) Mn/$AlPO_4$-11 with about 7 wt% of Mn.

shown in Fig. 3. In both cases the samples were calcined and then exposed to ambient conditions before the analysis. For Mn-11, contrasting with Mn-supported $AlPO_4$-11, the intensities of the side bands are strongly enhanced. A similar effect, noticed by Olender et al. [12] over a MnAPSO material, was attributed to anisotropic paramagnetic shift due to dipolar interaction of ^{31}P nuclei with paramagnetic Mn(II). In the present case this effect is more pronounced probably due to the higher Mn content of our sample as compared with the one used by the former authors (as much as 4 times).

The sample Mn-11 with the higher Mn loading showed a violet colour, contrasting with the pale-brown one showed by a Mn-impregnated $AlPO_4$-11. This indicates that Mn ions are in a chemical environment, when added to the synthesis gel, different from the one in the Mn-impregnated material.

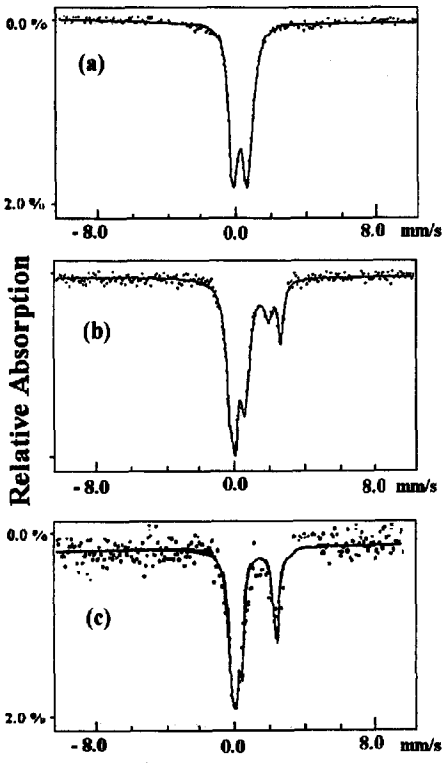

Fig. 4. Mossbauer spectra at room temperature of F-11 (a) calcined (b) as-synthesized and (c) after reaction with 1-butene at 743 K.

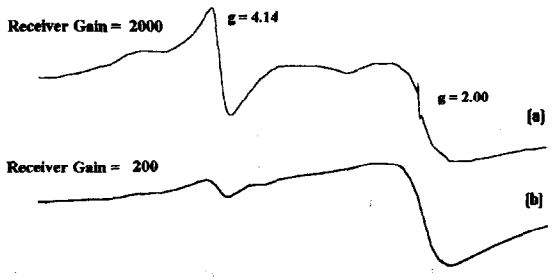

Fig. 5. X-band EPR spectrum of (a) as-synthesized F-11 and (b) calcined F-11.

The high proportion of weak Lewis acidity, observed for the Fe-containing sample, can be explained in terms of the presence of extra-framework Fe(III) after the calcination treatment. From the Mössbauer spectrum shown in Fig. 4a the characteristic doublet of Fe(III), probably as well-dispersed Fe_2O_3 particles in calcined F-11, can be observed. A typical Fe(II) doublet is absent, indicating that most of the Fe(II) initially present was oxidized. In fact, the spectrum of the as-synthesized F-11, shown in Fig. 4b, indicates that even before calcination Fe(III) is present. This spectrum was fitted into three doublets, two of them with isomer shifts at 1.44 and 1.13 mm/s are associated to Fe(II) and the third one, with an isomer shift at 0.29 mm/s is ascribed to Fe(III). The latter value is very close to the one previously obtained for Fe(III) in tetrahedral coordination in ordered crystalline materials [13]. Furthermore, EPR spectrum of F-11 before calcination (see Fig. 5a) showed a strong signal at $g_1 = 4.14$ that has been previously ascribed to tetrahedral Fe(III) and another one at $g_2 = 2.00$ related to octahedral Fe(III) [14]. The latter signal also showed a superimposed well-defined narrow signal, typical of a free-electron resonance, probably due to the presence of the organic template occluded in the solid. The g_2/g_1 signal-intensity ratio was close to unity (0.9). After calcination this ratio was increased to 5.8 (Fig. 5b), suggesting the segregation of structural Fe(III) to extra-framework positions. Moreover, the as-synthesized F-11 sample showed a dark-green colour contrasting with a brown-earth typical of Fe_2O_3

observed after calcination. Under reaction conditions, in the presence of hydrocarbons, partial reduction of Fe(III) to Fe(II) has been reported to occur [4]. In fact, when a sample of F-11 was made to react with 1-butene at 743 K the Mössbauer spectrum showed in Fig. 4c was obtained. In this case the Fe(II) doublet, in addition to the one associated to Fe(III), was clearly evidenced. Based on the previous observation a pyridine adsorption–desorption treatment, under similar conditions to those used for the acidity determination, was performed for F-11. A Mössbauer spectrum identical to the one corresponding to the calcined F-11, shown in Fig. 4a, was obtained, discarding the reduction of Fe(III) by this reagent. Consequently, the observed Brønsted acidity on this solid can not be associated to the 'in situ' reduction of Fe(III) to Fe(II) by pyridine in the AEL structure. Therefore, a different approach, considering the possibility that structural Fe(III) can generate surface acidity, is to be figured out. A model, taking into consideration such alternative is presented in Fig. 6. Initially, Fe atoms are thought to be incorporated in the structure of the as-synthesised material. Then, after calcination, most of the Fe species Fe(III) ions are dislodged from the framework to form well-dispersed and isolated Fe_2O_3 particles that would act as Lewis sites. This breakage of the structure would give rise to a structural charge imbalance, leading to a negatively charged framework and, consequently, to potential Brønsted acidity. Such a situation would result in a less crystalline material as was, indeed, observed (see Table 2). The Mössbauer spectrum of Fig. 4a is characteristic of Fe(III) either as ionic species or as well-dispersed isolated Fe_2O_3 particles. Moreover, the calculated isomer shift and quadrupole splitting parameters, 0.41 and 0.8 mm/s, respectively, are very close to those obtained by Cardile et al. [13] for an amorphous Fe-phase.

Chromium was the only metal generating strong acid sites of both, Lewis and Brønsted nature. This observation suggests a difference in the way the metals studied are interacting in the AEL framework to create acid sites. Chromium, in the as-synthesized Cr-11, is very likely to be incorporated as trivalent metal-ion in place of Al atoms. In such a situation the resulting solid must be electronically neutral. During the calcination treatment, as was previously proposed by Chen and Sheldon [5], Cr(III) in octahedral coordination within the framework with two additional water ligands, is thought to be oxidized to Cr(VI) in tetrahedral coordination as dioxochromium (VI) species, giving rise to a negatively charged framework that can be balanced by protons. These authors also found that incorporation of Cr(VI) species generate strong Lewis centres. A missing point of the model is related with the way in which electron donor molecules, such as pyridine, interact with Cr atoms without altering their tetrahedral coordination. In this respect, Janchen et al. [15] envisaged a sort of distorted tetrahedral for structural Co atoms to explain the observed Lewis acidity in CoAPO materials.

Evidence for the occurrence of Cr(III) in the as-prepared CrAPO was obtained from the UV/VIS-diffuse reflectance spectrum shown in Fig. 7a. From this spectrum, typical bands at 440 and 622 nm, ascribed to octahedral Cr(III) species [16] were clearly observed. After calci-

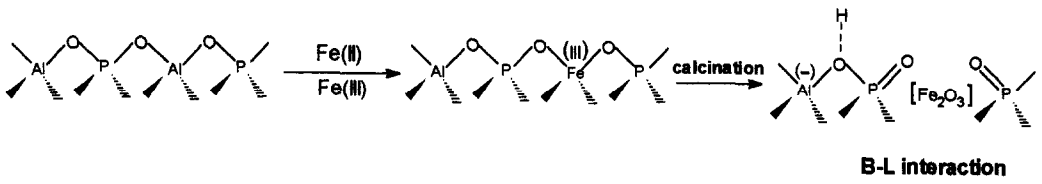

Fig. 6. Proposed model to explain how the incorporation of Fe(III) in the framework might generate, after calcination, surface acidity and Brønsted–Lewis interaction.

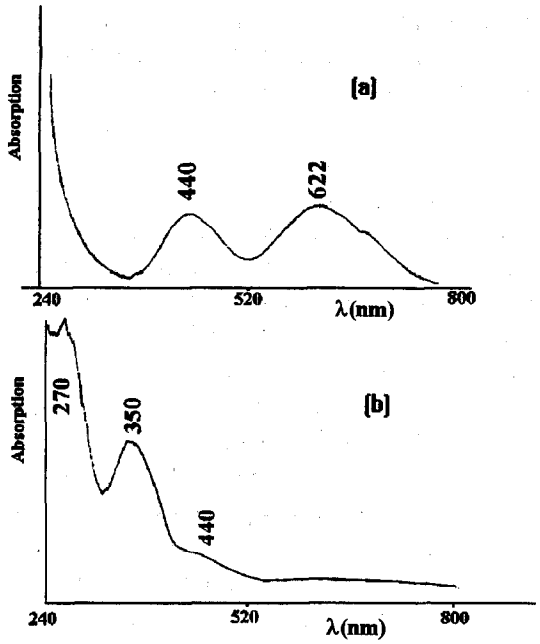

Fig. 7. DRS spectra of Cr-11: (a) as-synthesized and (b) calcined.

nation at 793 K under air stream, the DRS spectrum shown in Fig. 7b was obtained. In this case, main bands at around 270 and 350 nm, ascribed to Cr(VI) and a small shoulder at 440 nm, associated with Cr(III), were observed.

The above discussion finds support in the fact that the crystal field stabilization energy (CFSE) for octahedral Cr(III) (224.5 kJ/mol) is much higher than the one for tetrahedral Cr(III) (66.9 kJ/mol) [17]. For Cr(VI), on the contrary, tetrahedral coordination has been shown to be preferred [18].

The addition of chromium to the synthesis gel of SAPO-11, led to a solid (CrS-11) with an increased proportion of moderate and strong acid sites with respect to the SAPO-11 free of chromium. This is in good agreement with the expected generation of such kind of sites, resulting from the mechanism of chromium incorporation already discussed. On the contrary, Cr-impregnated SAPO-11 (sample Cr/S-11) showed a reduction of moderate and strong sites and a significant increase of weak sites as compared to the basic SAPO solid. These differences in the acidic properties of the samples Cr/S-11 and CrS-11 further suggest the incorporation of chromium in the AEL framework when added to the synthesis media.

Recent characterization studies on the chromium system using XPS and redox cycles [19] as well as adsorption of NO, acidity measurements on reduced and oxidic materials, DRS and the skeletal isomerization of 1-butene [20,21] have been reported. For the sake of completion and due to the relevance of these studies, a summary of the salient features is reproduced:

(1) DRS and XPS studies showed that a large fraction of Cr(VI) was found on the oxidic CrS-11 sample. XPS showed that almost 70% of the chromium existed as Cr(VI). A large amount (~ 82%) of Cr(III) was found for the oxidic Cr-supported material (Cr/S-11), Chemisorption of NO showed the presence of high chromium oxidation states on the oxidic CrS-11, thus, agreeing with the DRS and XPS results [19]. The distribution of oxidation states of chromium for the reduced CrS-11, derived from XPS and NO chemisorption, was different (~ 40% Cr(VI) and ~ 60% Cr(III)) compared to the oxidic sample. These results show that Cr(VI) was more stable towards reduction at (H_2, 773 K) in the CrS-11 catalyst, compared to Cr-supported on conventional supports e.g. alumina and zirconia. The difficulty in reducing the Cr(VI) species supports the notion of incorporation of chromium into the framework. For the Cr/S-11 solid, Cr(III) was extremely stable towards oxidation at 773 K and almost no differences were observed for the distribution of oxidation states of chromium for the oxidic and reduced catalysts. Due to the redox characteristics and the values for the Cr 2p/ Al 2p intensity ratios, the formation of chromia species on this catalyst is suggested. The above mentioned XPS results showed excellent agreement with redox data (H_2–O_2) cycles.

(2) As already mentioned, the oxidic CrS-11 catalyst showed an increase in the number of moderate and strong acid sites compared to its SAPO-11 counterpart. The reduction process,

however, decreased the strong Brønsted acid sites by a factor of two. A concomitant decrease was observed for the moderate and strong Lewis acid sites upon reduction [19]. These results suggest that a partially unsaturated Cr(VI) in the vicinity of OH groups may act as strong Lewis sites, enhancing Brønsted acidity by Brønsted–Lewis interaction. After the reduction process the number of Cr(VI) species is considerably decreased, lowering not only the Lewis but also the Brønsted acidity. On the contrary, the supported sample showed a reduction of moderate and strong acid sites compared to the SAPO-11 matrix. In this case, the reduction process did not cause major changes in the acidity distribution.

(3) The CrS-11 catalyst was more selective towards the formation of isobutene, for times-on-stream < 2.5 h, than its SAPO-11 counterpart and the supported chromium system [19]. After 2.5 h a drastic decrease in the selectivity occurred with a concomitant increase in the formation of butadiene and 2-butenes. Changes in acidity brought about by the reduction process of the Cr(VI) species (in the CrS-11) by the hydrocarbon stream may explain the differences, in accordance with the above discussion. No such effect was observed for the supported system.

(4) To further evaluate the feasibility of incorporation of Cr(VI) into the framework, successive ion exchange treatments of the calcined CrS-11 sample with an ammonium nitrate solution were performed. The results showed almost no loss of Cr(VI) from the calcined material. It is well known [5] that nonframework Cr(VI) species are easily extracted from calcined related materials by simply treating them with water.

In order to verify the relationship between Brønsted and Lewis sites suggested by the models already discussed, Brønsted acidity, expressed as the intensity of the B-band after outgassing at 623 K, was plotted in Fig. 8a against the L-band intensity at the same evacuating temperature. As seen, there is a very good

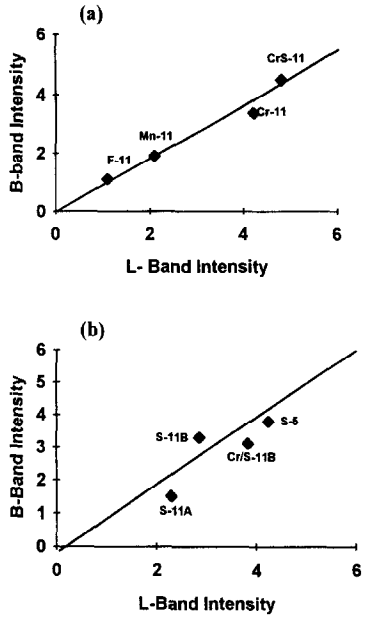

Fig. 8. Correlation between Brønsted and Lewis site population for substituted $AlPO_4$ molecular sieves after pyridine removal at 623 K: (a) MeAPO's and MeAPSO and (b) SAPO's.

linear correlation between them, with a slope close to unity ($B = 0.09 + 0.85L$; $r = 0.98$), strongly supporting a one-to-one Lewis–Brønsted interaction, as predicted by the above described models. Interestingly, Mn and Fe incorporation led to acid sites of the same acid strength (weak and moderate) whereas the trivalent incorporation of chromium followed by oxidation to Cr(VI) gave rise to stronger acid sites. In would seem that the electron acceptor capacity (Lewis strength) of the metal ion in the framework, governs the resulting acid strength of the combined-site. In fact, the strong electron-withdrawal character of the free oxygen atoms linked to Cr atoms is expected to increase the electron accepting capacity of the metal centre.

Si-containing materials (SAPO), as we have already reported [3], have also shown the same kind of correlation between Brønsted and Lewis acid sites. Such correlation can be visualized in Fig. 8b. Interestingly, although the linear correlation observed for these samples, adjusted by least-square ($B = -0.11 + 0.92L$; $r = 0.83$), is not as good as the one obtained for the metal-

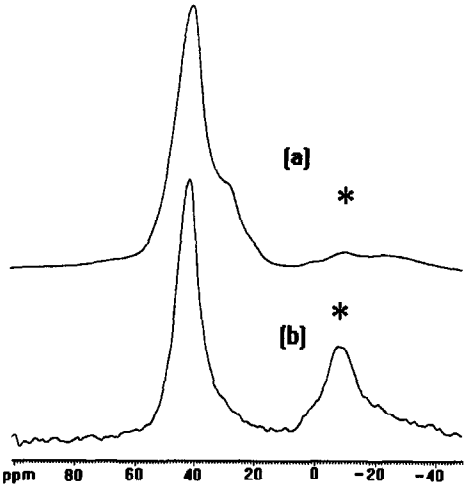

Fig. 9. Solid state MAS NMR spectra of S-11B (a) ^{27}Al MAS NMR and (b) ^{1}H–^{27}Al CP/MAS NMR. Band assigned to Al^{VI}, has been labeled with an asterisk.

containing series (MeAPO and MeAPSO), the resulting slope close to unity suggests, again, a one-to-one Lewis–Brønsted interaction. In order to explain this curious synergism a situation in which a small fraction of the original Al–O bonds (those adjacent to Si atoms) would break down to generate defective electron-deficient species, might be imagined. These electron-acceptor species would be interacting with Brønsted-like OH groups giving rise to new sites of enhanced acidity, as has been classically proposed in the literature for silicoaluminate materials [22].

The ^{27}Al MAS NMR spectrum of a calcined and exposed to ambient SAPO sample is shown in Fig. 9a. A small band at around -15 ppm, in addition to the main one at around 40 ppm (corresponding to framework tetrahedral Al in $AlPO_4$ environment), was clearly observed. This band is more evident from Fig. 9b, in which ^{1}H–^{27}Al CP/MAS NMR spectrum is shown. Previous reports [23,24] have ascribed this band to framework octahedral Al atoms. The fact that ^{1}H–^{27}Al CP/MAS NMR experiments showed an intensity enhancement of this band strongly supports the association of these octahedrally coordinated Al atoms with either water molecules or OH groups. A similar band was ascribed by Janchen et al. [24] to octahedrally coordinated framework Al atoms after water and NH_3 adsorption experiments on $AlPO_4$-18 at around 300 K.

3.2. Catalytic properties

A summary of the catalytic results is presented in Table 4. In spite of the fact that the total conversion of 1-butene remained almost constant at around 80% regardless of the nature of the catalyst, strong differences in the skeletal isomerization selectivity were observed. It follows that the double-bond isomerization is a facile reaction that readily occurs under the actual reaction conditions over these materials. Under these circumstances a mixture of *n*-butenes can be considered as the actual pool of reactants for the skeletal rearrangement. $AlPO_4$-11 (A-11) showed a very low skeletal isomerization and negligible amounts of undesirable by-products, in line with its low Brønsted acidity and in spite of possessing moderate + strong Lewis sites. The incorporation of additional elements in the AEL framework gave rise to an increase of the SIE which correlates with the medium + strong acidity of both Brønsted and Lewis kind, as can be observed from Fig. 10. As derived from this figure the Cr-supported sample Cr/S-11B does not fit these correlations. This sample, as determined by previous studies [20] whose summary has already been presented, is very likely to contain free chromia. Since the accessibility of pyridine and 1-butene seems not to have been restricted by the pres-

Table 4
Summary of the catalytic results for the transformation of 1-butene at 743 K after 30 min on-stream

Sample	X	S_c	S_{C5+}	S_{db}	S_{si}	S_b	SIE
A-11	0.78	0.006	0.004	0.95	0.04	0.005	0.08
S-11A	0.78	0.03	0.02	0.71	0.24	0.002	0.55
S-11B	0.83	0.04	0.06	0.54	0.37	0.001	0.87
F-11	0.76	0.005	0.005	0.84	0.15	0.003	0.33
Mn-11	0.84	0.01	0.01	0.70	0.28	0.001	0.62
CrS-11	0.82	0.10	0.05	0.44	0.37	0.05	0.96
Cr/S-11B	0.82	0.01	0.02	0.80	0.16	0.005	0.36

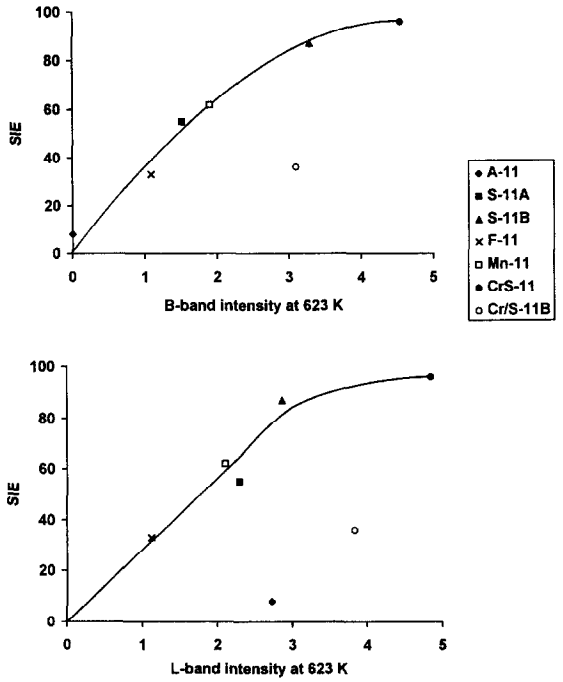

Fig. 10. Correlation between the skeletal isomerization efficiency (SIE) and the pyridine IR-band intensity measured after outgassing at 623 K. (a) Brønsted band and (b) Lewis band.

ence of this material and the fact that the active sites for the double-bond isomerization were not affected, a sort of a selective deactivation of the medium + strong acid sites, thought to be the active centres for the skeletal rearrangement, has to be considered. The sample A-11 neither fit the correlations, particularly the one for the Lewis acid sites. This observation indicates that Lewis sites alone can not act as active centres for this reaction. However, a few sites with the strength enough to catalyse the skeletal isomerization have to be accepted to exist on A-11 in order to explain the experimental observation. The nature of these sites might be envisaged, as suggested by Gielgens et al. [4], as weakly acidic OH-groups interacting with Lewis acid centres. It is well known that olefins adsorption is highly enhanced in the presence of Lewis centres. Therefore, in addition to its electron-withdrawal effect on the lability of the adjacent proton, a Lewis centre in the vicinity of a Brønsted one will also favour the necessary adsorption step of the reactant.

The solid CrAPSO showed the highest SIE (96%) in agreement with its highest acid strength. Selectivity towards butadiene was also the highest (5%) suggesting the presence of a dehydrogenating species [20,21]. As was already referred, Cr(VI) species initially present in the calcined CrS-11 can be reduced by hydrogen [19]. It is also well known that chromium containing catalysts can be reduced by hydrocarbons [25]. Thus, such partially 'in situ' reduced chromium species may act as dehydrogenating sites as suggested in a recent literature report [25]. In previous work [21] we had already reported the dramatic loss of skeletal isomerization selectivity, after 150 min on-stream, for the CrAPSO-11 catalyst. The absence of butadiene when Cr-supported SAPO (Cr/S-11) was used, further strengthens its differences with CrAPSO-11 and reinforces the idea of the formation of free chromia (non-dehydrogenating species) on this sample. Further discussion on this matter can be found in a work sent for publication [20]. It seems that the closer to the equilibrium yield for isobutene the higher the cracking and C_5^+ production. A similar observation was reported over ZSM-22 by Corma et al. [8]. This product enhancement seems to occur at the expense of the 2-butenes produced (cis- and trans-2-butenes). Probably, olefin oligomerization followed by cracking of the oligomers formed is likely to be favoured at near-equilibrium ($C_4=$) conditions. Furthermore, the higher the acid site (medium + strong) population the higher the extension of these consecutive transformations should be. A more detailed product distribution study, out of the scope of this work, should be done to draw any definitive conclusion.

4. Conclusions

Incorporation of Si and metal ions in the aluminophosphate framework generates, after calcination, acid sites of both Lewis and Brønsted type of enhanced acid strength compared to their parent unsubstituted $AlPO_4$. A

clear synergism between these two kind of acid sites are likely to occur, leading to solids of improved catalytic activity. This idea of a Lewis–Brønsted synergism has long been considered for zeolites and related materials. So, Mirodatos and Barthomeuf [26] proposed the existence of 'superacid sites' consisting of extra-framework Al species acting as Lewis centres interacting with structural OH sites. This model was first experimentally proved by Dwyer et al. on a series of steam-treated ZSM-5 zeolites [27]. More recently, Su and Barthomeuf [28] also suggested that the increase in acid strength of a SAPO-37 sample upon heating, might be related to an interaction between protons and Lewis centres.

From the characterization study of the metal-containing solids, particularly for the chromium system, the incorporation of the metals studied seems to occur. The resulting acidity strongly depends on both the oxidation state and the stability of the metal species in the framework. Models advanced in the literature to explain the acidity generation after Me(II) [4] and Cr(III) [5] incorporation, have been used to rationalise our results.

The skeletal isomerization efficiency during the transformation of 1-butene correlates well with both Lewis and Brønsted sites of medium and high acid strength. Lewis sites alone can not act as active centres for such skeletal rearrangement. Differences in the catalytic behaviour of CrAPSO-11 as compared with Cr/SAPO-11 support the idea of structural Cr species existing in the former and extra-framework chromia occurring in the latter.

Acknowledgements

This work was supported by CONICIT project RPI 10.001. Mössbauer spectra were taken in 'Laboratorio de Magnestismo, Facultad de Ciencias, UCV'. Acknowledgement is also due to Dr. C. Forte from 'Instituto di Chimica Quantistica ed Energetica Molecolare', CNR, Pisa, Italy, for ^{1}H–^{27}Al CP/MAS NMR experiments.

References

[1] D. Barthomeuf, Zeolites 14 (1994) 394.
[2] M. Makarova, A. Ojo, K. Al-Ghefaili, J. Dwyer, Proc. 9th Int. Zeolite Conference, Vol, II (1992) p. 259.
[3] M. Alfonzo, J. Goldwasser, C.M. López, F.J. Machado, M. Matjushin, B. Méndez, M.M. Ramirez de Agudelo, J. Mol. Catal. 98 (1995) 35.
[4] L. Gielgens, I. Veestra, V. Ponec, M. Haanepen, J. van Hooff, Catal. Lett. 32 (1995) 195.
[5] J. Chen, R. Sheldon, J. Catal. 153 (1995) 1.
[6] A.V. Kucherov, A.A. Slinkin, G.K. Beyer, G. Boberly, Zeolites 15 (1995) 431.
[7] H. Mooiweer, K. de Jong, B. Kraushaar-Czametzki, W. Stork, B. Kruttzen, Stud. Surf. Sci. Catal. 84 (1995) 2327.
[8] M. Asensi, A. Corma, A. Martinez, J. Catal. 158 (1996) 561.
[9] H. Zubowa, M. Richter, U. Roost, B. Parlitz, R. Fricke, Catal. Lett. 19 (1993) 67.
[10] M. Guisnet, P. Andy, N. Gnep, E. Benazzi, C. Travers, J. Catal. 158 (1996) 551.
[11] J. Martens, P. Grobet, P. Jacobs, J. Catal. 126 (1990) 299.
[12] Z. Olender (Levi), D. Goldfarb, J. Batista, J. Am. Chem. Soc. 115 (1993) 1.106.
[13] C. Cardile, N. Tapp, N. Milestone, Zeolites 10 (1990) 90.
[14] H. Li, J. Martens, P. Jacobs, S. Schubert, F. Schmidt, H. Zeithen, A. Trautwein, Stud. Surf. Sci. Catal. 37 (1988) 75.
[15] J. Janchen, M. Peeters, J. Van Wolput, J. Wolthuizen, J. Van Hooff, U. Lohse, J. Chem. Soc. Faraday Trans. 90 (1994) 1033.
[16] B. Weckhuysen, R. Schoonheydt, Zeolites 14 (1994) 360.
[17] A.R. West, Basic Solid State Chemistry (Wiley, Chichester, 1988).
[18] M.A. Vuurman, Y.E. Wachs, J. Phys. Chem. 96 (1992) 5008.
[19] L. Giraldo, C. Pfaff, C.M. López, F.J. Machado, B. Méndez, J. Goldwasser, M.M. Ramirez de Agudelo, S. Rondón, M. Houalla, D.M. Hercules, Surf. Int. Anal., 24 (1996) 863.
[20] D. Escalante, L. Giraldo, C. Pfaff, V. Sazo, M. Matjushin, M. Pinto, B. Méndez, C.M. López, F.J. Machado, J. Goldwasser, M.M. Rarmirez-Agudelo, J. Catal., in press.
[21] D. Escalante, C.M. López, F.J. Machado, M. Matjushin, B. Méndez, M. Pinto, M.M. Ramirez-Agudelo, in: G. Centi et al. (Eds.), Environmental Catalysis, 1st World Conference (SCI, Rome, 1995) p. 415.
[22] J. Lunsford, J. Phys. Chem. 72 (1968) 4163.
[23] H. He, J. Klinowski, J. Phys. Chem. 97 (1993) 10.385.
[24] J. Janchen, M.P.J. Peeters, J.W. de Haan, L.J.M. van de Ven, J.H.C. van Hooff, Y. Gimus, U. Lohse. J. Phys. Chem. 97 (1993) 12.042.
[25] A. Hakuli, A. Kytökivi, O.Y. Krause, T. Suntola, J. Catal. 161 (1996) 393.
[26] C. Mirodatos, D. Barthomeuf, J. Chem. Soc. Chem. Commun. (1981) 29.
[27] A.G. Ashton, S. Batmanian, D.M. Clark, J. Dwyer, F.R. Fitch, A. Hinchcliffe, F.J. Machado, Stud. Surf. Sci. Catal. 20 (1985) 101.
[28] B. Su, D. Barthomeuf, J. Catal. 139 (1993) 84.